

Supplementary Information

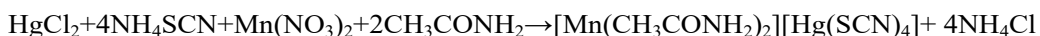
Bulk Crystal Growth and Optical Properties of Novel Organic-inorganic Hybrid Nonlinear Optical Thiocyanate: [Mn(CH₃CONH₂)₂] [Hg(SCN)₄]

Peiqing Long^a, Chunli Hu^a, Xitao Liu^a, Jianggao Mao^{a,b,*}

- a. State Key Laboratory of Functional Crystals and Devices, Fujian Institute of Research on the Structure of Matter, Chinese Academy of Sciences, Fuzhou, Fujian 350002, China. Email: mjg@fjirsm.ac.cn
b. University of Chinese Academy of Sciences, Beijing 100049, China.

Experiment

Synthesis and Crystal Growth. MMTA was synthesized via a one-step reaction procedure of HgCl_2 , NH_4SCN , $\text{Mn}(\text{NO}_3)_2$ and acetamide, in a ratio of 1:4:1:2 in deionized water at room temperature according to the subsequent chemical equation:



The initial material underwent two rounds of recrystallization to achieve a high level of purity necessary for crystal growth. Single crystals were cultivated using the temperature reduction technique. Carefully selected crystal seeds, obtained through spontaneous nucleation, were immersed in a solution that had reached its saturation point. The growth process commenced at approximately 45°C. Initially, the saturated solution was filtered and maintained at a temperature 10°C above its saturation point for several hours. The rate at which the temperature was lowered started at 0.2 °C per day and gradually increased as the crystals continued to grow. Bulk single crystals with dimensions of 50×50×12 mm³ were successfully obtained were grown within 30 days.

Crystal structure determination. The crystal structure data of MMTA crystal was obtained using a single crystal X-ray diffractometer (Bruker D8) with Mo K α radiation ($\lambda = 0.71073 \text{ \AA}$) at a temperature of 300 K. The structures were determined through direct methods and refined using the full matrix least-squares method based on F^2 , utilizing the SHELXL software package. Anisotropic refinement was performed for all non-hydrogen atoms, while the positions of hydrogen atoms in organic moieties were generated geometrically.

Linear and Nonlinear Optical Properties. UV-Vis-NIR optical transmission spectrum of MMTA crystal was measured using a Hitachi U-3500 recording spectrophotometer at room temperature. The crystal had a thickness of 1.2 mm, and the measurements were conducted within the wavelength range of 200-3200 nm. For analyzing powder SHG, we utilized a modified Kurtz-NLO system. It is widely acknowledged that particle size affects the efficiency of SHG in powders. Hence, we individually ground MMTA crystals and sieved them into distinct particle size ranges: 20-44, 45-89, 90-149, 150-211, 212-249, and 250-360 μm . To enable relevant comparisons with known SHG materials, crystalline KH_2PO_4 (KDP) was also ground and sieved into identical particle size ranges as the MMTA crystals. Our experimental setup for measuring NLO properties involved employing a high-power Mode-Locked Nd:YAG laser (M200) emitting pulses lasting for 200 ps at a repetition rate of 5 Hz. We selected a measurement wavelength of 1064 nm for our analysis purposes. One part of our setup focused on capturing SHG signals in the sample while another part generated signals in the reference material (KDP pellet).

Theoretical Calculations. Theoretical calculations were conducted using single crystal XRD data of MMTA. The CASTEP code^{1, 2} was utilized to conduct band structure and density of states (DOS) analysis, employing the Perdew-Burke-Ernzerhof functional for solids (PBESOL)³ within the framework of generalized gradient approximation in density functional theory (DFT). Norm-conserving pseudopotentials were employed to describe the interactions between ionic cores and electrons⁴. Valence electrons considered in this study included Mn 4d⁵ 5s²; Hg 5d¹⁰ 6s², C 2s² 2p², N 2s² 2p³, S 3s² 3p⁴, O 2s² 2p⁴ and H 1s¹. A cutoff energy of 830 eV was utilized to determine the inclusion of plane waves in the basis sets, while numerical integration of the Brillouin zone was facilitated through Monkhorst-Pack κ -point sampling with a size of 3×3×1. The default values provided by the CASTEP code were employed for all other parameters and convergent criteria.

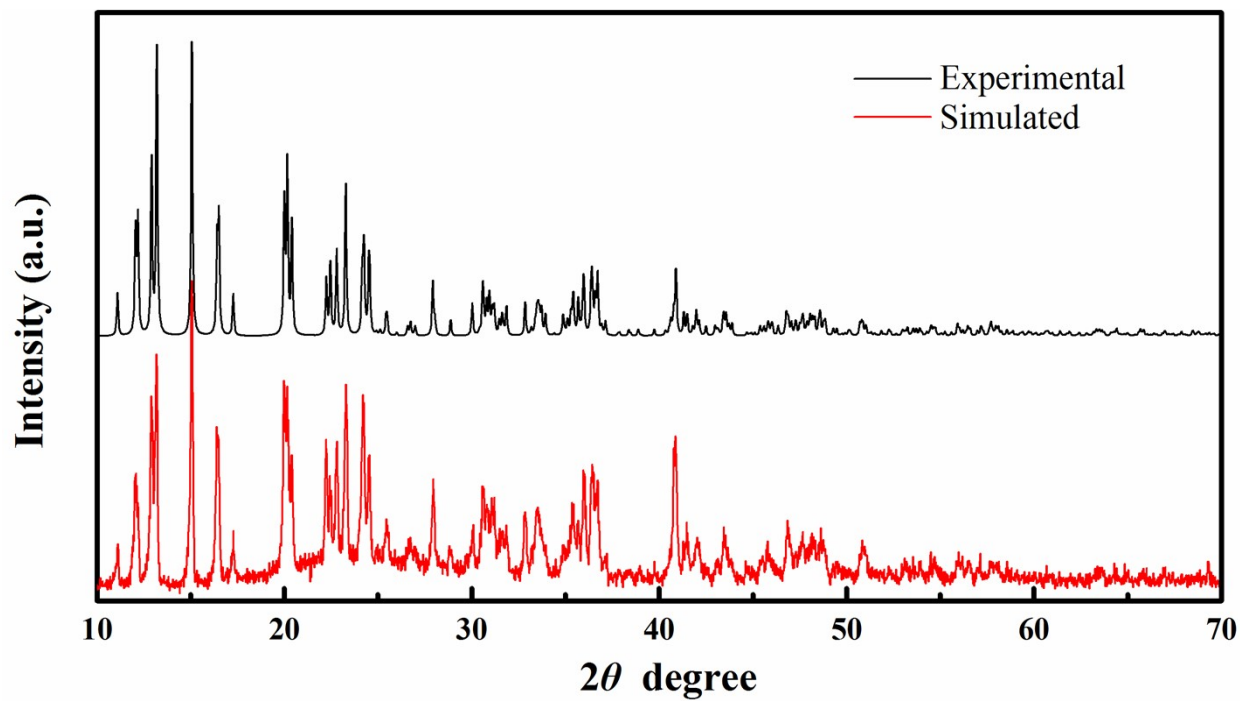


Figure S1 Experimental and calculated XRD patterns of $[\text{Mn}(\text{CH}_3\text{CONH}_2)_2][\text{Hg}(\text{SCN})_4]$ crystal.

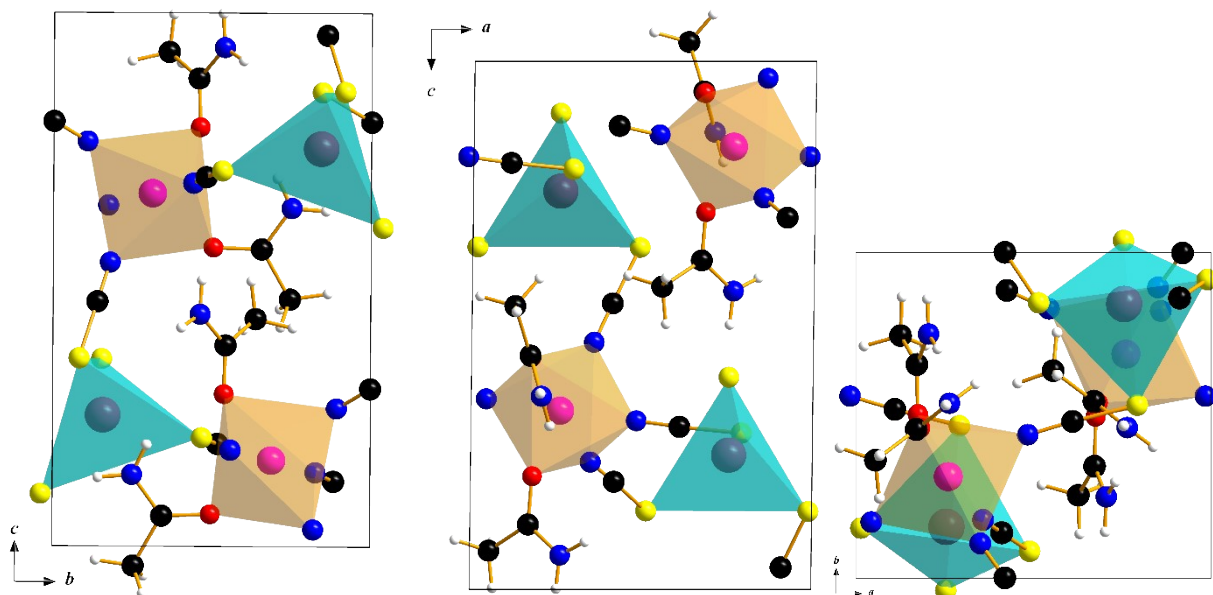


Figure S2 Packing diagram of $[\text{Mn}(\text{CH}_3\text{CONH}_2)_2][\text{Hg}(\text{SCN})_4]$ crystal viewed along *a*, *b* and *c* axis, respectively.

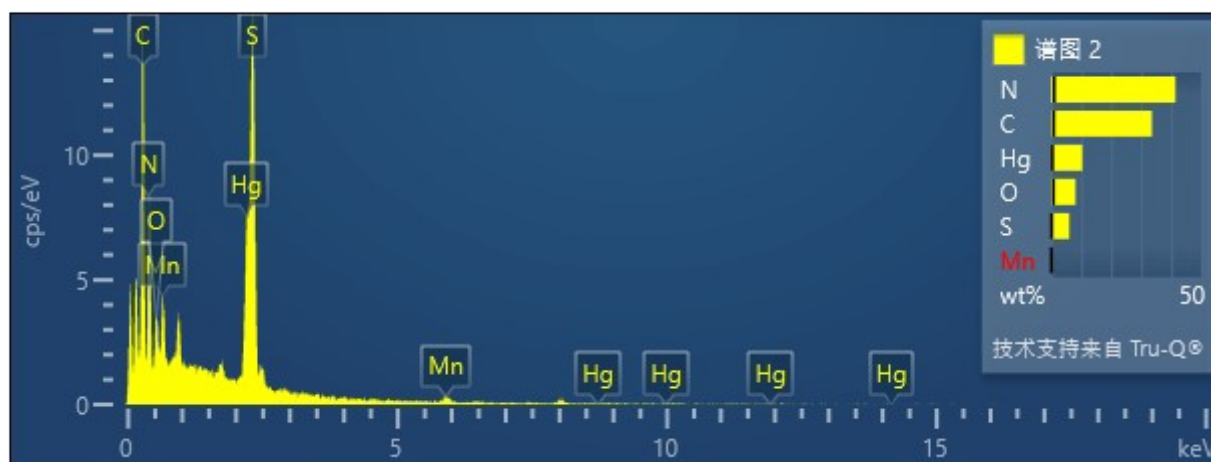
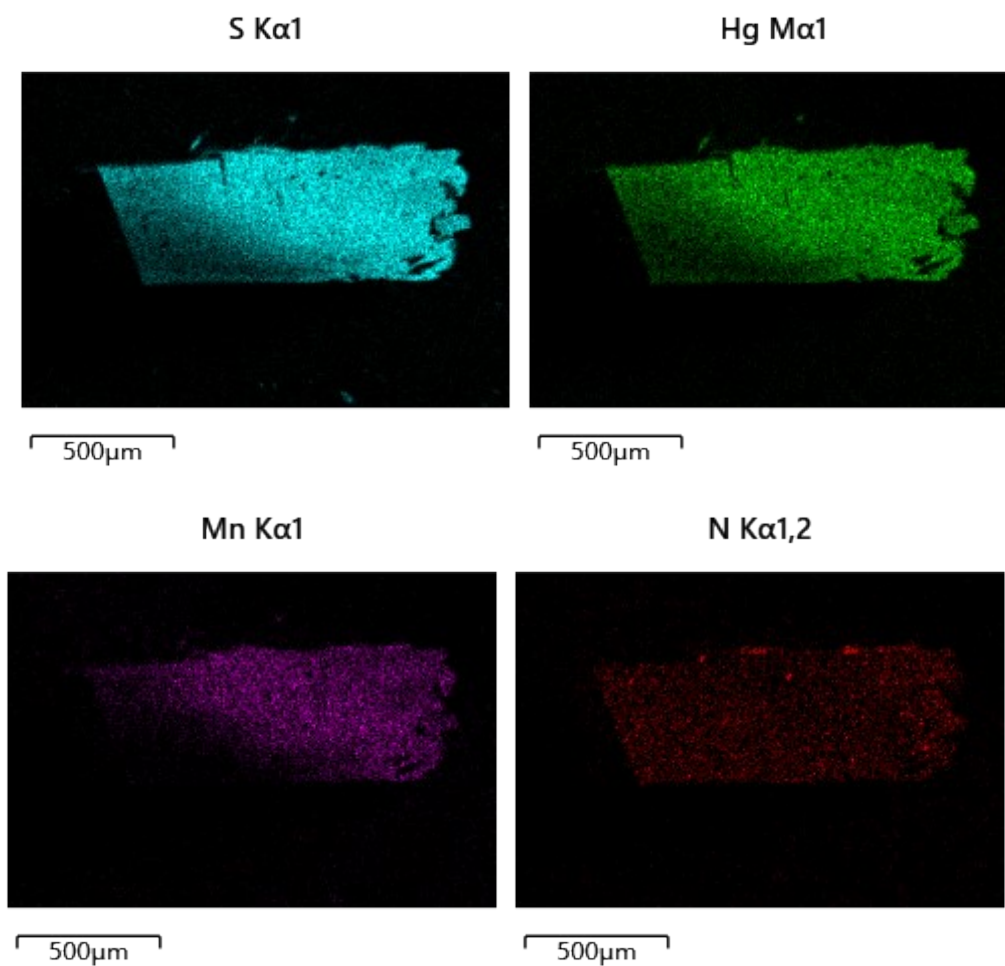


Figure S3 The energy-dispersive spectroscopy (EDS) mapping of $[\text{Mn}(\text{CH}_3\text{CONH}_2)_2][\text{Hg}(\text{SCN})_4]$ crystal.

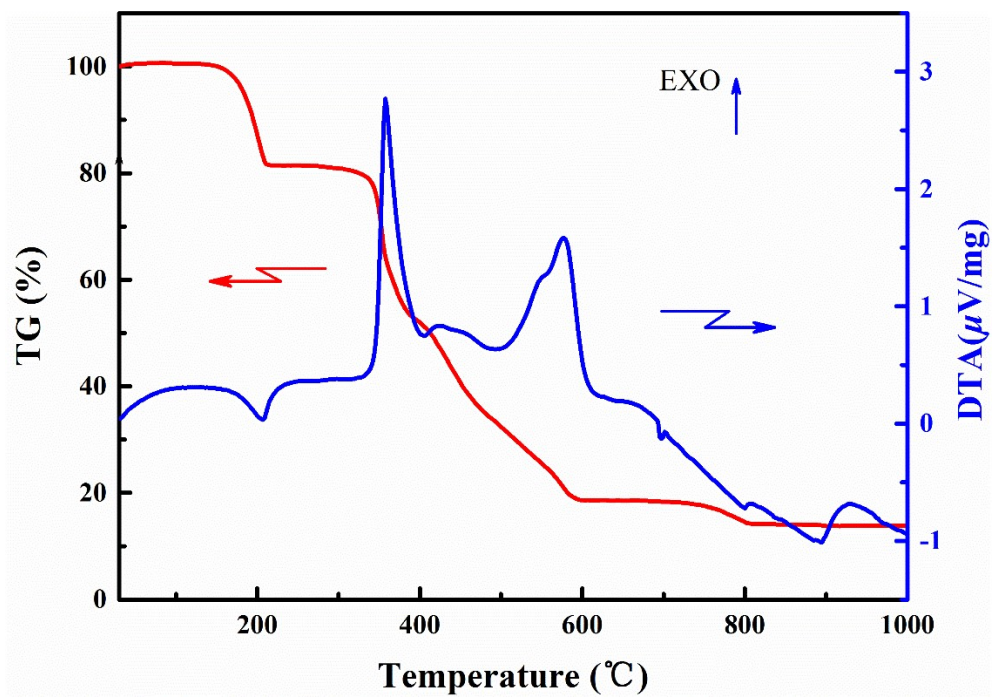


Figure S4 TGA/DTA curves of $[\text{Mn}(\text{CH}_3\text{CONH}_2)_2][\text{Hg}(\text{SCN})_4]$ crystal in air.

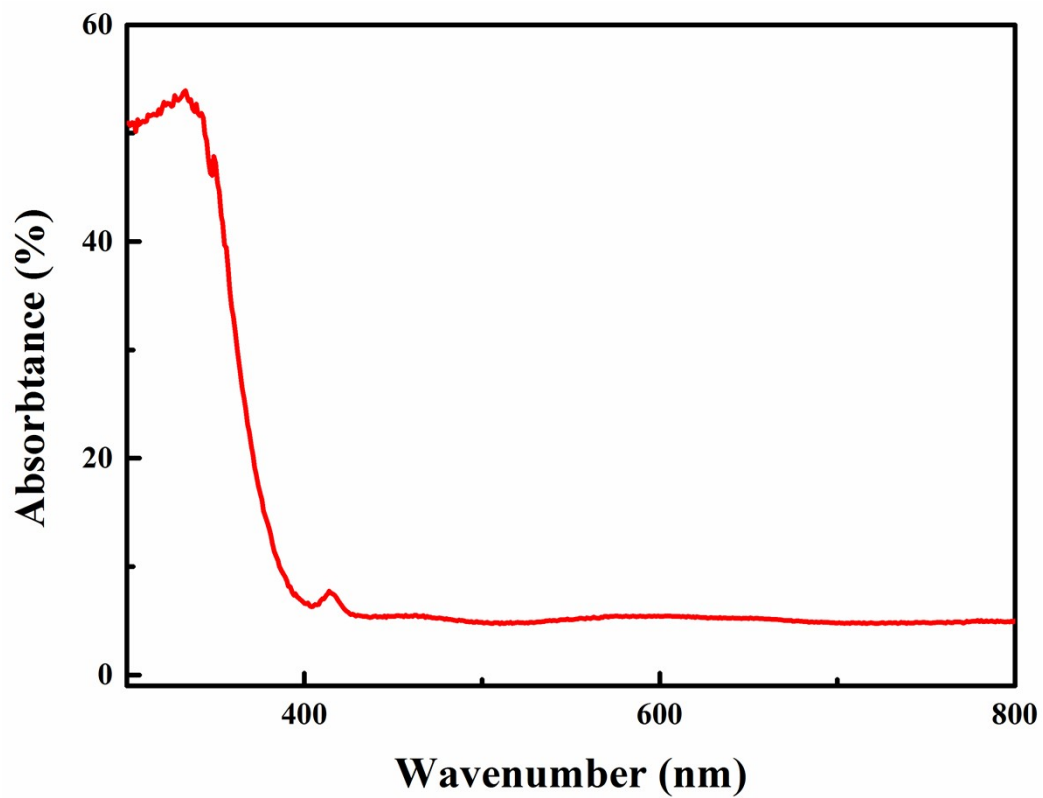


Figure S5 UV/Vis absorption spectra of [Mn(CH₃CONH₂)₂][Hg(SCN)₄] crystal.

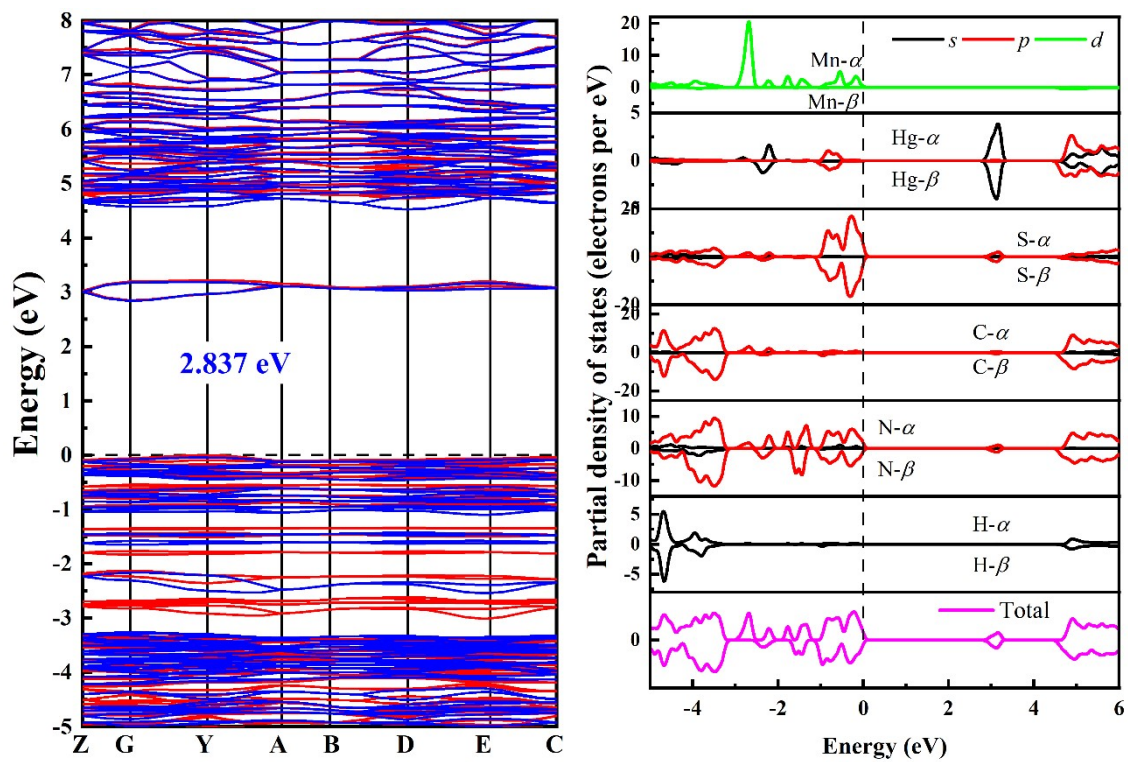


Figure S6 Energy band structure (a) and partial density of states (PDOS) (b) of $[\text{Mn}(\text{CH}_3\text{CONH}_2)_2][\text{Hg}(\text{SCN})_4]$ crystal near the Fermi level.

Reference

1. M. D. Segall, P. J. D. Lindan, M. J. Probert, C. J. Pickard, P. J. Hasnip, S. J. Clark and M. C. Payne, First-principles simulation: ideas, illustrations and the CASTEP code, *J. Phys.: Condens. Matter*, 2002, **14**, 2717-2744.
2. S. J. Clark, M. D. Segall, C. J. Pickard, P. J. Hasnip, M. J. Probert, K. Refson and M. C. Payne, First principles methods using CASTEP, *Zeitschrift Fur Kristallographie*, 2005, **220**, 567-570.
3. J. P. Perdew, A. Ruzsinszky, G. Csonka, I. Bor, O. A. Vydrov, G. E. Scuseria, L. A. Constantin, X. Zhou and K. Burke, Restoring the Density-Gradient Expansion for Exchange in Solids and Surfaces, *Phys. Rev. Lett.*, 2008, **100**, 136406.
4. D. R. Hamann, M. Schlüter and C. Chiang, Norm-Conserving Pseudopotentials, *Phys. Rev. Lett.*, 1979, **43**, 1494.